

In: Image Fusion
Editor: C. T. Davis, pp. 45-81

ISBN: 978-1-63482-115-5
© 2015 Nova Science Publishers, Inc.

No part of this digital document may be reproduced, stored in a retrieval system or transmitted commercially in any form or by any means. The publisher has taken reasonable care in the preparation of this digital document, but makes no expressed or implied warranty of any kind and assumes no responsibility for any errors or omissions. No liability is assumed for incidental or consequential damages in connection with or arising out of information contained herein. This digital document is sold with the clear understanding that the publisher is not engaged in rendering legal, medical or any other professional services.

Chapter 3

FUSION OF MULTIFOCUS COLOR IMAGES FROM MICROSCOPIC SAMPLES USING THE MODULUS OF THE GRADIENT OF THE COLOR PLANES

Carina Toxqui-Quitl, Román Hurtado-Pérez,
Alfonso Padilla-Vivanco and Gabriel Ortega-Mendoza*
Universidad Politécnica de Tulancingo, División de Ingenierías,
Calle Ingenierías, Tulancingo, Hidalgo, México

Abstract

Commonly in the light microscopy, the limited Depth-of-Field (DOF) of an imaging system causes blur images when the sample is wider than the DOF of the optical system. Additionally, the DOF decreases as the magnification increases. In order to extend the DOF of a microscopic system we propose a multifocus image fusion method based on the modulus of the gradient color planes. This procedure is applied to multi-focus microscopy color images which have been acquired by the bright-field reflection microscopy technique. Our results are obtained using real specimens and any post-processing step is done over the fused image. The proposed method is simple, fast and practically free of artifacts or false color.

*E-mail address: carina.toxqui@upt.edu.mx

PACS: 05.45-a, 52.35.Mw, 96.50.Fm

Keywords: Multifocus Image fusion, gradient color operator, depth of field, optical microscopy

AMS Subject Classification: 53D, 37C, 65P

1. Introduction

In general, focusing is a procedure of adjusting the distance between an optical system and its image plane until a contrast-enough image is reached. Focusing cameras is an important problem in computer vision and microscopy, due to the limited depth of field (*DOF*) of some optical systems. Particularly, images of thick objects acquired by using a microscope system are strongly blurred in the portion of the object that lies outside of the depth of field of the microscope objective lens. This means that, only small regions of the field of view are in-focus. In order to overcome this problem some techniques such as wavefront coding [1][2] and image fusion [3] [4] have been proposed.

Typically, many digital techniques have been proposed to generate fusion schemes. These fusion schemes are divided in (a) pixel-based image fusion [5], (b) neighborhood-based image fusion [6] and multiresolution image fusion [7][8]. It is well know that, image fusion schemes have been broadly used in many context such as in optical microscopy [9], medical imaging [10], hyperspectral [11] and pancromatic imaging [12], anti-tank landmine detection [13], and many others applications.

Currently, image fusion allows merging images from multiple sensors or even multiple images from the same sensor [14][15][10]. Its goal is to integrate complementary information to provide a composite image which could be used to better understanding of the entire scene. A common found problem can be to fuse multifocus images, which are acquired from optical imaging systems. The challenge is to obtain a resulting fused image that contains enough-sharp information.

Generally, a current solution in multifocus image fusion is to reconstruct an image of the whole specimen by acquiring multi-focus images corresponding to each focused plane of the sample. The important thing is to find from each slice-image the region that is better focused in order to obtain an overall fused image with enough contrast in all the field of view. As we will see in this chapter, the digital image fusion methods take different in-focus parts of a sample and

digitally or numerically combine them into a single composite image which contains the entire focused scene.

Many works have been published related with multifocus image fusion schemes. However, the main amount of these papers work with monochromatic input images to get a final fused image. Only a few of them have proposed the fusion of multifocus color images, and less common in the particular application of using microscopic samples [3][6][16].

In this chapter, we have proposed a new method of fusion of color images by pixels based on the Modulus of the Gradient Color planes (*MGC*) [17][18]. This algorithm requires the computation of the gradient for each image-channel from a *RGB* image. The procedure is fast and generate high sharply fusion images. The main application of our method is in the context of optical microscopy. The microscopic samples used in this chapter are metallic and biological with several textures and with irregular surfaces.

This chapter is organized as follows: in section 2, it is described the modulus of the gradient of color planes algorithm. This algorithm is the core of the method. Section 3 is used to explain the image fusion scheme step by step. Experiments and image acquisition are described in section 4. In the section 5, the fusion results including fused images are shown. Finally, in section 6 a discussion of the results and the conclusions of the method performance are included.

2. The Modulus of the Gradient of the Color Planes (MGC)

It is not unknown that in the *RGB* space, color vectors of Red, Green and Blue components are related to each pixel of a *RGB* image, which is commonly given by,

$$\mathbf{C}(x, y) = R(x, y)\hat{i} + G(x, y)\hat{j} + B(x, y)\hat{k}, \quad (1)$$

where $R(x, y)$, $G(x, y)$, and $B(x, y)$ are the *RGB* space channels and \hat{i} , \hat{j} , and \hat{k} the unitary direction vectors.

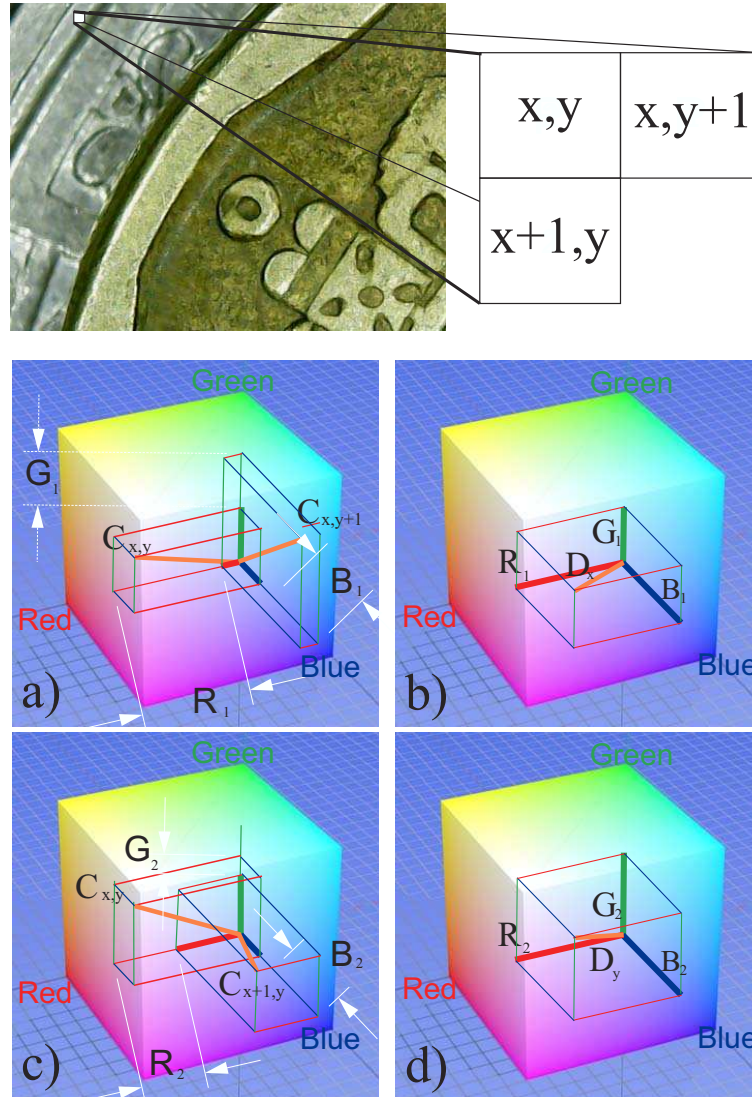


Figure 1. Modulus of the Gradient Color operator $|MGC[C(x, y)]|$ obtained by taking the Euclidean distance between color vectors.

A compound gradient image $I_C^g(x, y) = |MGC[C(x, y)]|$ can be reconstructed from the resulting images of the gradient modulus of $|\nabla R|$, $|\nabla G|$, and $|\nabla B|$. This compound image can be calculated by [19][20],

$$I_C^g(x, y) = \sqrt{\left(\frac{\partial R}{\partial x}\right)^2 + \left(\frac{\partial G}{\partial x}\right)^2 + \left(\frac{\partial B}{\partial x}\right)^2 + \left(\frac{\partial R}{\partial y}\right)^2 + \left(\frac{\partial G}{\partial y}\right)^2 + \left(\frac{\partial B}{\partial y}\right)^2}. \quad (2)$$

In general, the modulus of the gradient of the color planes I_C^g , is computed using the Euclidean distance as [18],

$$I_C^g(x, y) = |MGC[C(x, y)]| = \sqrt{\sum_{i=1}^{band} \left[\left(\frac{\partial C(x, y, i)}{\partial x}\right)^2 + \left(\frac{\partial C(x, y, i)}{\partial y}\right)^2 \right]}, \quad (3)$$

where $i = 1, \dots, band$ is the dimensionality of the color space and $|MGC[C(x, y)]|$ is the color gradient operator. In the particular case of working with the *RGB* space, $band = 3$ is used. A vectorial sketch of computation of the modulus of the gradient color planes is shown in the Figures 1 and 2.

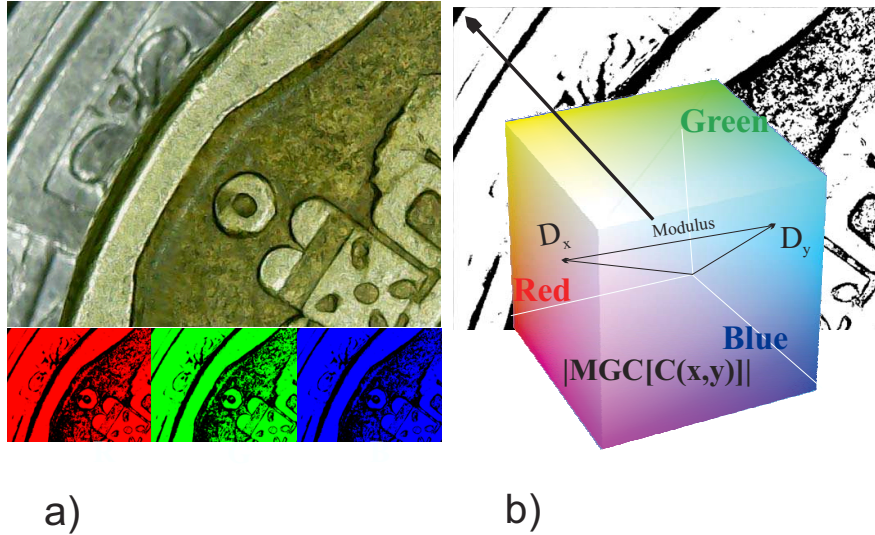


Figure 2. (a) Input color image and (b) MGC edge map.

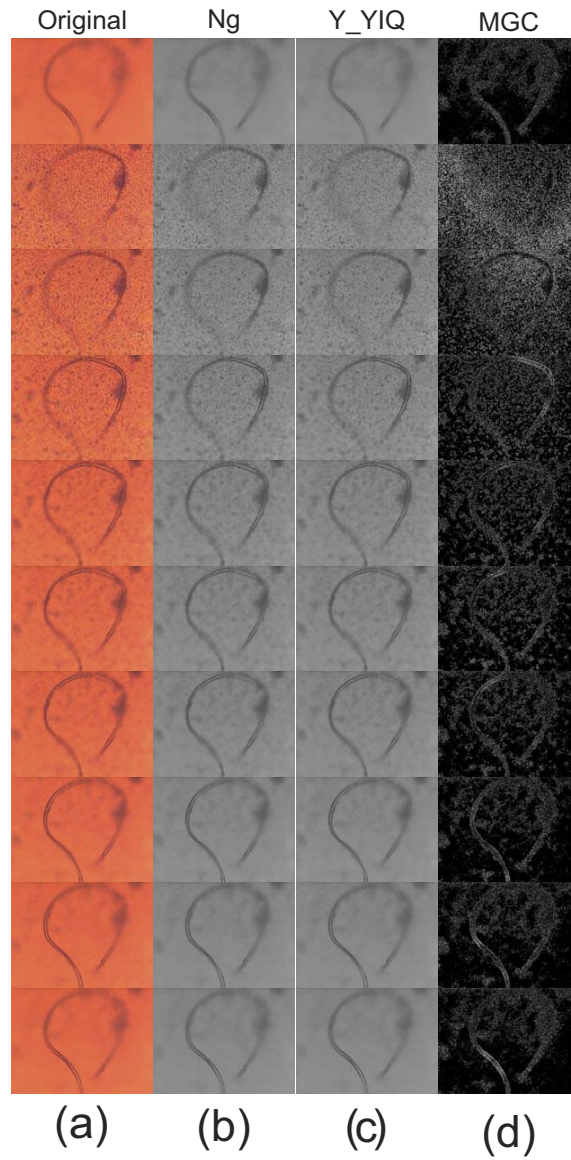


Figure 3. (a) Input color images, (b)intensity channel, (c) Y channel from the YIQ color space, and MGC edge map of (a).

Currently, the partial derivative along the x - axis of a two-dimensional function $C(x, y, i)$ can be approximated by the difference,

$$\frac{\partial C(x, y, i)}{\partial x} \approx C(x, y, i) - C(x + 1, y, i), \quad (4)$$

in a similar way, the partial derivative along the y - axis is given by,

$$\frac{\partial C(x, y, i)}{\partial y} \approx C(x, y, i) - C(x, y + 1, i). \quad (5)$$

Therefore, the modulus of the gradient color planes is an edge map that can be computed by the expression,

$$I_C^g(x, y) = \sqrt{\sum_{i=1}^{band} [(C(x, y, i) - C(x + 1, y, i))^2 + (C(x, y, i) - C(x, y + 1, i))^2]}. \quad (6)$$

In the Figure 3, the edges on an individual image directly in the color vector space are shown.

3. Image Fusion Scheme

Extended DOF in microscopy systems can increase the quantity of reachable most structural details available in thick specimens. Extended DOF have been obtained using different digital fusion methods. In this section, we propose a new approach to extended DOF through the modulus of the color gradient planes. We can start this section by establishing some definitions of the proposed method.

Let $C_j(x, y, i)$ be a z - stack of N input color images, where $j = 1, \dots, N$. The index $i = 1, \dots, band$ represents the color channel. In order to highlight the details in the input images, we have used sharpening spatial filters known as Sobel H_k^S , Prewitt H_k^P , Kirsch H_k^K , and Frei-Chen $\frac{1}{2\sqrt{2}}H_k^F$. The four filters are shown in the Figure 4 and the $m \times n$ size in the Figure 5.

Therefore, a sharpening version $g_j(x, y, i)$ of the input color image $C_j(x, y, i)$ is reconstructed by the maximum pixel values from each k filtered image $C_j^k(x, y, i)$ as follows,

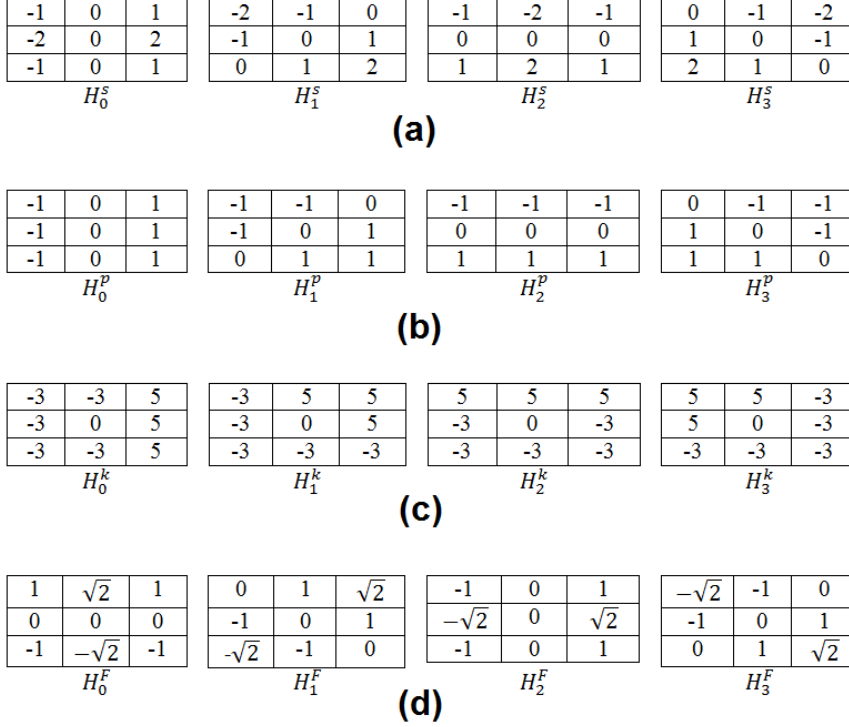


Figure 4. (a) Sobel, (b) Prewitt (c) Kirsch and (d) Frei-chen filters in the four cardinal directions.

$$F_j(x, y, i) = \max_k [C_j^k(x, y, i)]. \quad (7)$$

Now, we can define a new fusion scheme Φ given by,

$$\Phi(x, y, i) = \begin{cases} C_1(x, y, i), & |MGC[F_1(x, y, i)]| \geq |MGC[F_2(x, y, i)]|, \\ C_2(x, y, i), & \text{otherwise.} \end{cases} \quad (8)$$

where $|MGC[F_j(x, y, i)]|$ is the modulus of the color gradient planes of $F_j(x, y, i)$ for $j = 1, 2$; which can be computed by Ec. (6). Schematically the image fusion procedure is shown in the Figure 6.

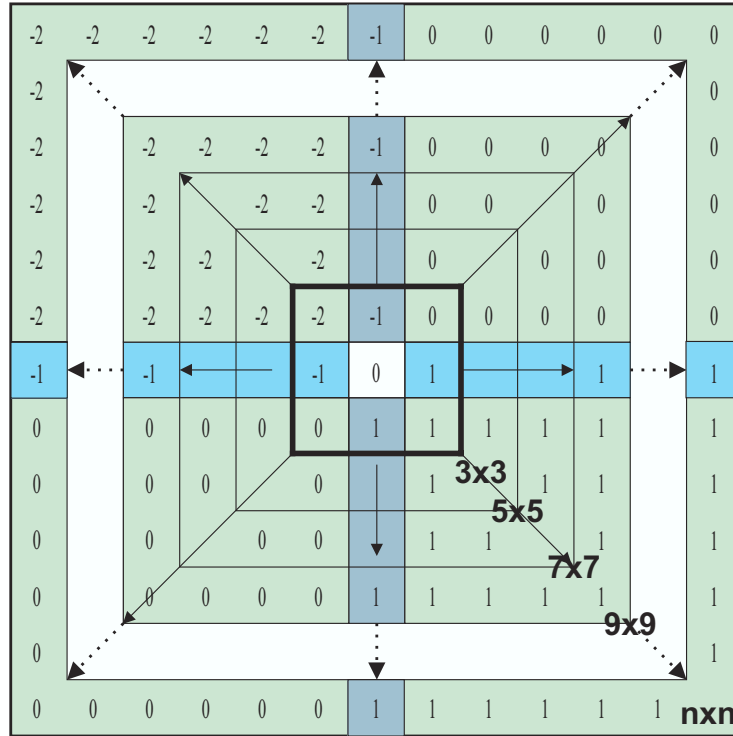


Figure 5. Sobel filters in the four cardinal directions for different sizes.

In order to measure the performance of the fusion algorithm, we have implemented the mean μ of the $\Phi(x, y, i)$ of the color fused image as follows,

$$\mu = \sum_{x=0}^{M-1} \sum_{y=0}^{N-1} MGC[\Phi(x, y, i)]. \quad (9)$$

This last value is related with the contrast of a color fused image.

4. Image Acquisition and Experiments

A motorized microscope Carl Zeiss Axio Imager M1 is used for the image acquisition of the biological test samples. This system contains an integrated

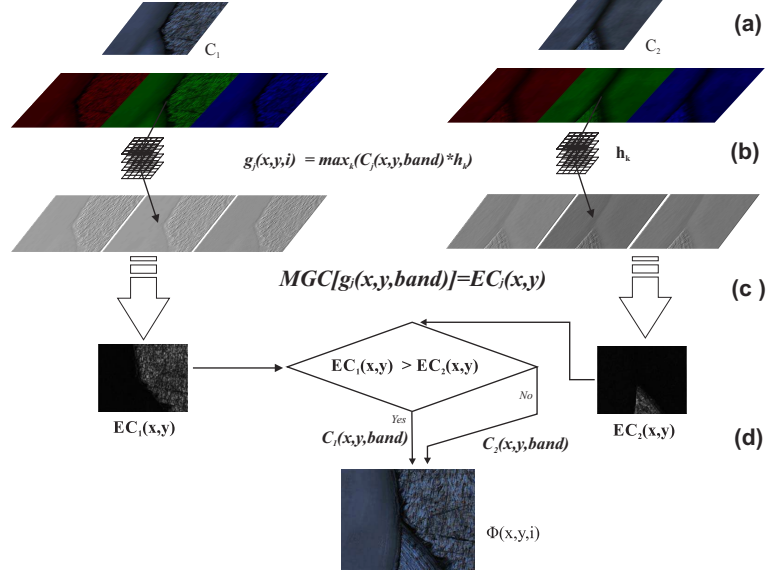


Figure 6. Steps of the fusion scheme. (a) input color images $C_j(x, y, i)$ where $j = 1, 2$, (b) sharpening version $g_j(x, y, i)$ of the input color images, (c) modulus of the color gradient operator of $g_j(x, y, i)$, (d) fusion rule based on the maximum pixel values from $|MGC[F_j(x, y, i)]|$.

AxioCam Mid Range Color camera of 5 megapixels with an image resolution of 2584 (H) \times 1936 (V) pixels and a pixel size of 8.7mm \times 6.6mm. The microscope make uses of a $x - y$ platform where the sample is located and a motorized stage to control the $z - focus$ position is employed. The numerical aperture NA and the magnification M of the objectives of the microscope system used during the experiment are related according with the Table 1. This parameters will be used for the determination of the depth variation z .

The depth-of-focus $\Delta z'$ in the monochromatic case is defined as follows [21],

$$\Delta z' = \frac{n\lambda}{(NA)^2}, \quad (10)$$

where λ is the wavelength of the light and n the refractive index. The relation

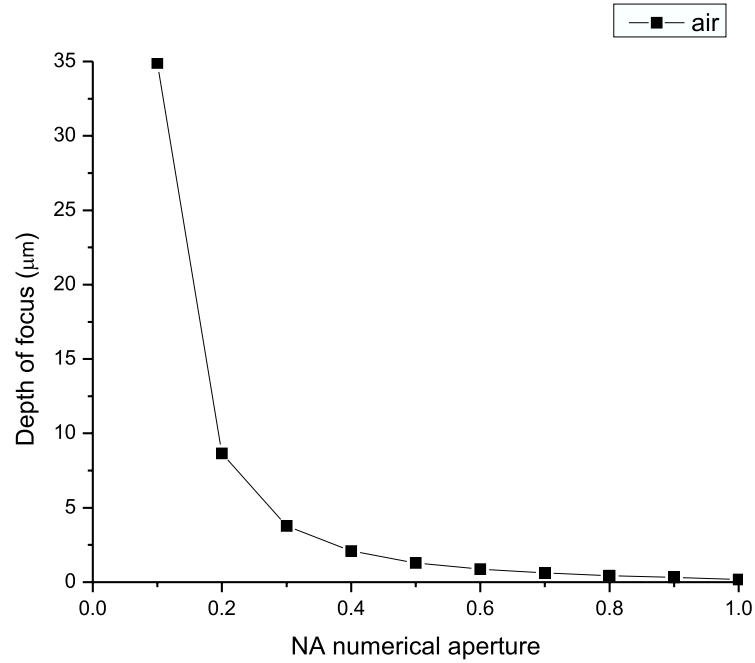


Figure 7. The depth-of-focus versus the NA.

Table 1.

Objective magnification	Numerical Aperture	Δz (DOF)
2.5X	0.16	50 micras
10X	0.30	20
40X	0.75	3
60X	0.9	2
100X	0.9	1

between depth-of-field Δz and depth-of-focus $\Delta z'$ is given by [21],

$$\Delta z' = M_{objective}^2 \Delta z \frac{n'}{n}, \tag{11}$$

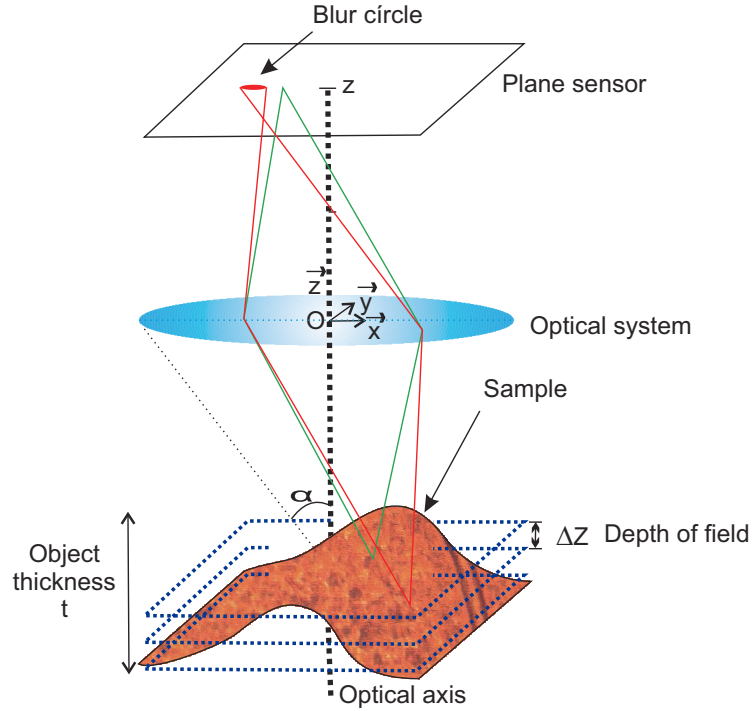


Figure 8. Microscopic imaging system.

where n' and n are, respectively, the media refractive indexes in the object and in the image space. The numerical aperture NA and magnification M are related by the following formula,

$$M = cteNA, \quad (12)$$

and

$$NA = n\sin(\alpha). \quad (13)$$

where α is the angular semi-aperture on the objective side. As we can see, in Figure 7 when the numerical aperture is increased, the depth of focus becomes smaller. For the case of the DOF , it is sketched in the Figure 8.

In order to measure the effectiveness of our proposed algorithm, the Figure 9 shows a stack of slice-images of some real samples illuminated by means of the bright-field technique and at different z depth positions, with $z < \Delta z$.

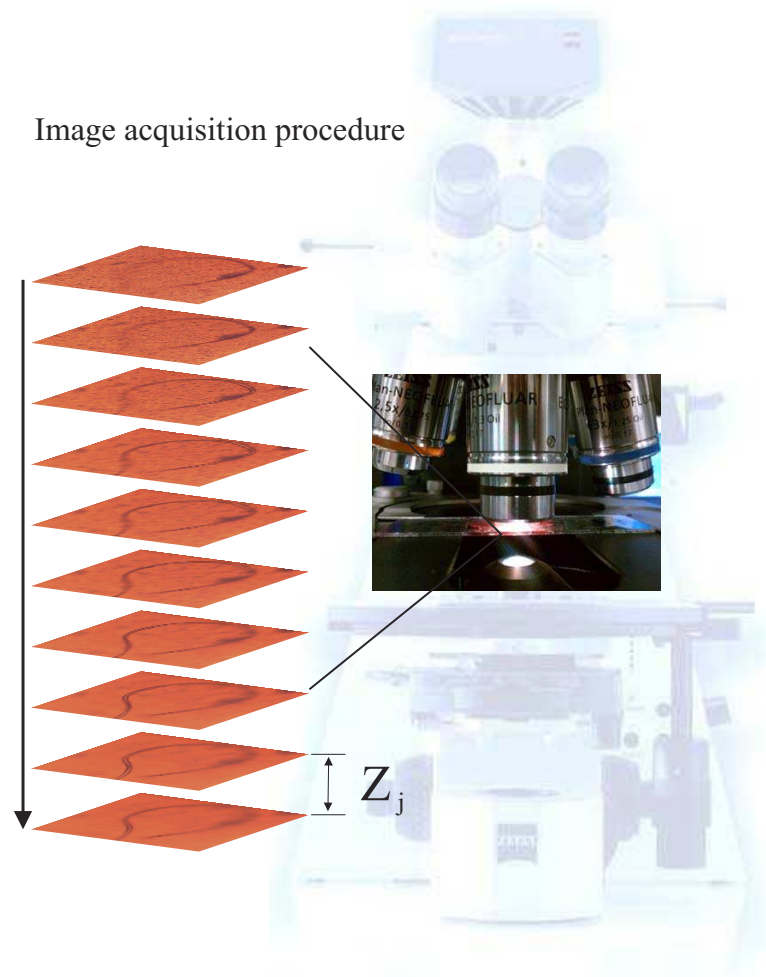


Figure 9. A z -stack of color slice-images from a biological sample which are acquired using the bright-field illumination technique at different z -depth positions.

5. Fusion Results

The digital color images which are taken from different focus planes of biological and metallic samples are shown in the Figures 10 and 11.

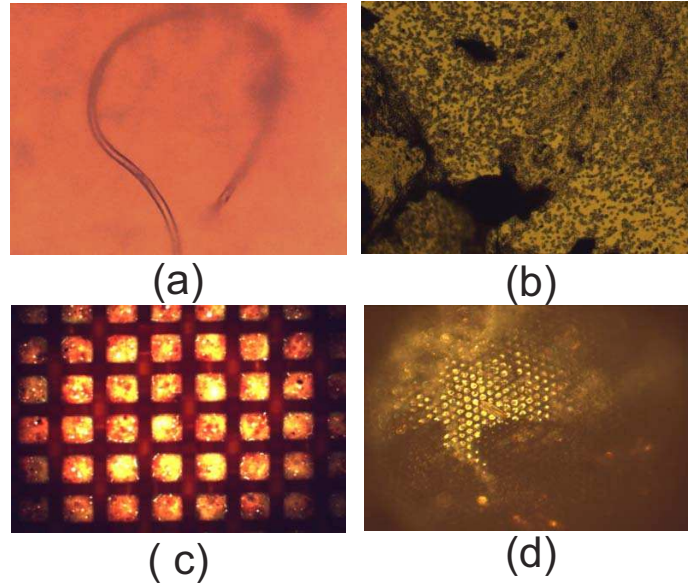


Figure 10. Test images acquired from biological samples of (a) bacillus of yogurt, (b) amniotic fluid, (c) tape to measure the glucose levels, and (d) bee eye. They are amplified by different objectives from amplifications of $10X$, $20X$, and $40X$ and $NA = 0.3$, 0.5 , and 0.75 respectively.

In this part we analyze the effectiveness of using the fusion scheme implemented for multifocus color images. In our first case, the biological sample is a bacillus of yogurt. Digital images of a bacillus of yogurt are acquired at $M = 40X$, $NA = 0.75$, and an axial distance of $z = 3\mu m$ between the two focal planes. The fusion results using the enhancement MGC edge map with different sharpening filters are shown in the Figures 12 to 13.

In the second example, images of the same bacillus of yogurt are acquired but using the amplification $M = 10X$, and $NA = 0.3$. An axial distance of $z = 3\mu m$ between the three focal planes is considered. The fusion results using the enhancement MGC edge map with different sharpening filters are shown in the Figures 14 and 15.

In the third case the bacillus of yogurt is now acquired at $M = 20X$, $NA = 0.5$, and an axial distance of $z = 3\mu m$ between ten focal planes. The fusion results using the enhancement MGC edge map with different sharp-

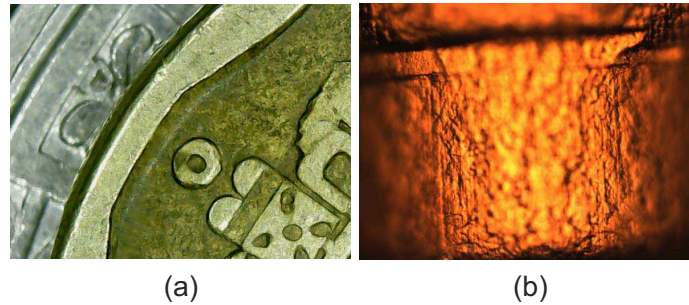


Figure 11. Test images acquired from metallic samples. They are amplified by different objectives from amplifications of $10X$, $20X$, and $40X$. The numerical apertures are from 0.3, 0.5, and 0.75 respectively. (a) coin, and (b) cylindrical piece of metal.

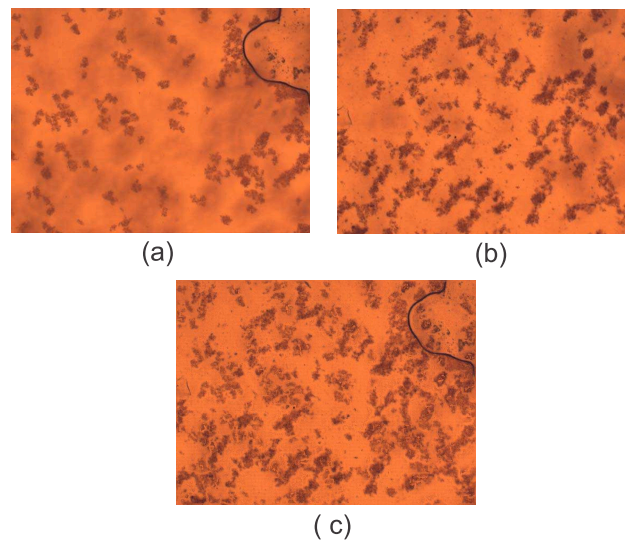


Figure 12. Bacillus of yogurt images acquired at $M = 40X$, $N.A. = 0.75$, and an axial distance of $z = 3\mu m$ between the two focal planes. (a) focal plane A, (b) focal plane B, and (c) Result of image fusion using the proposed enhancement MGC edge map.

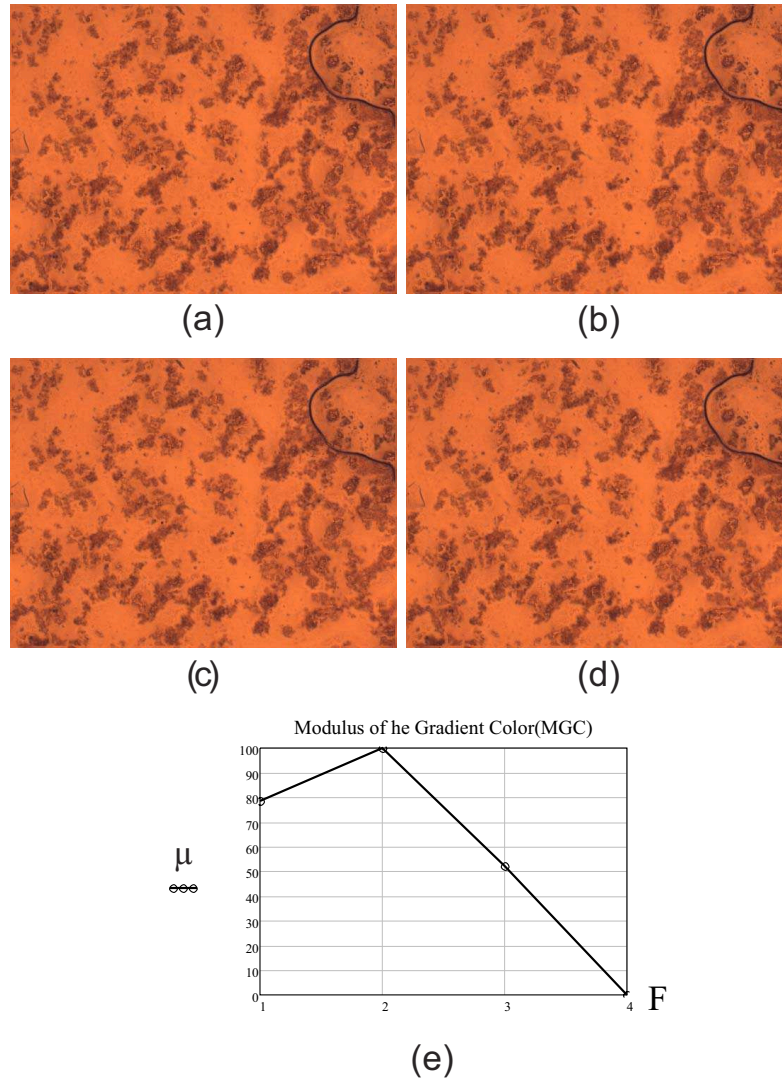


Figure 13. Results of image fusion using the proposed enhancement MGC edge map with the sharpening filters of (a) Frei-Chen (F=1), (b) Kirsch (F=2), (c) Prewitt (F=3), and (d) Sobel filter (F=4). (e) The results shown that the enhancement MGC edge map with Kirsch filter gives a major contrast fused image.

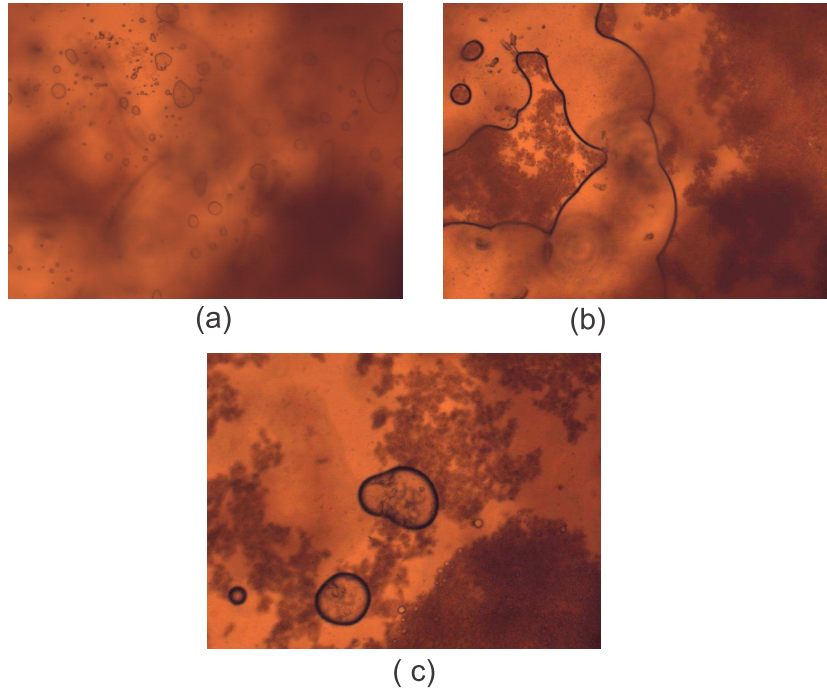


Figure 14. The sample is a bacillus of yogurt. The images are acquired at $M = 10X$, $N.A. = 0.3$, and an axial distance of $z = 3\mu m$ between the three focal planes. (a) focal plane A, (b) focal plane B, and (c) focal plane C.

ening filters are shown in the Figures 16 to 17. A major contrast fused image is obtained using the Kirsch filter.

An image of amniotic fluid is acquired at $M = 10X$, $N.A. = 0.3$, and an axial distance of $z = 10\mu m$ between the two focal planes. The fusion results using the enhancement MGC edge map with different sharpening filters are shown in the Figures 18 to 19. A major contrast fused image is obtained using the Kirsch filter.

An image of a tape to measure the glucose levels is acquired at $M = 10X$, $N.A. = 0.3$, and an axial distance of $z = 10\mu m$ between the two focal planes. The fusion results using the enhancement MGC edge map with different sharpening filters are shown in the Figures 20 to 21. A major contrast fused image is obtained using the Kirsch filter.

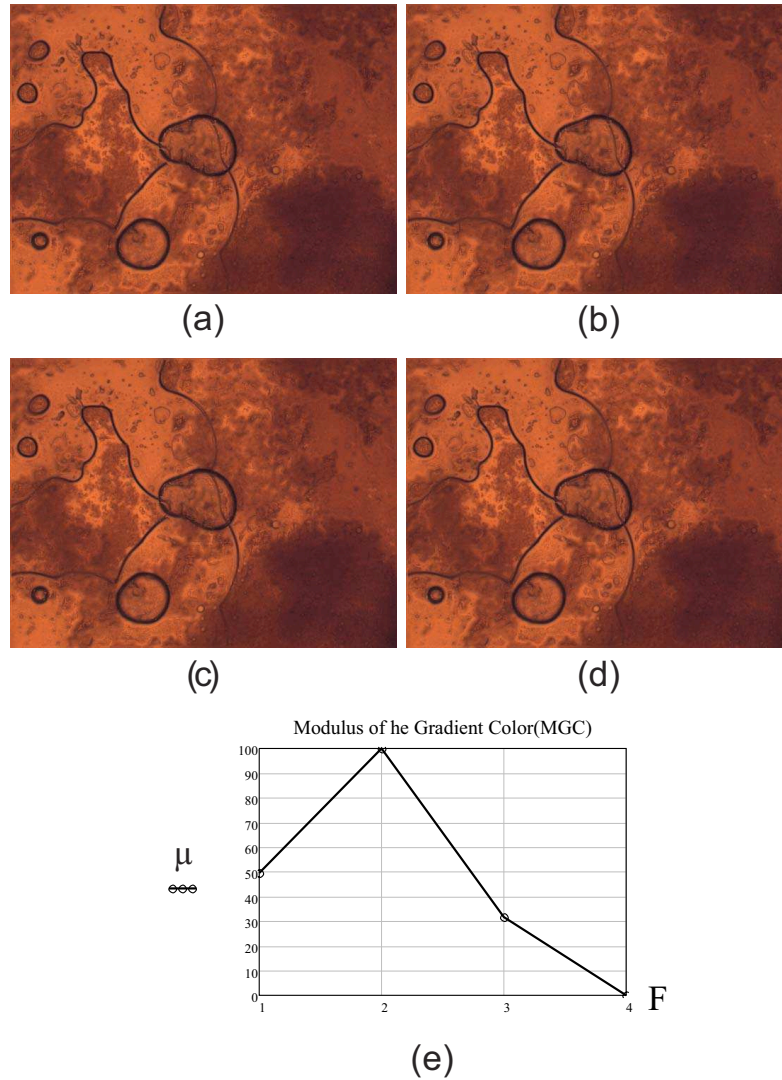


Figure 15. Results of image fusion using the proposed enhancement MGC edge map with the sharpening filters of (a) Frei-Chen (F=1), (b) Kirsch (F=2), (c) Prewitt (F=3), and (d) Sobel filter (F=4). The results shown that the enhancement MGC edge map with Kirsch filter gives a major contrast fused image.

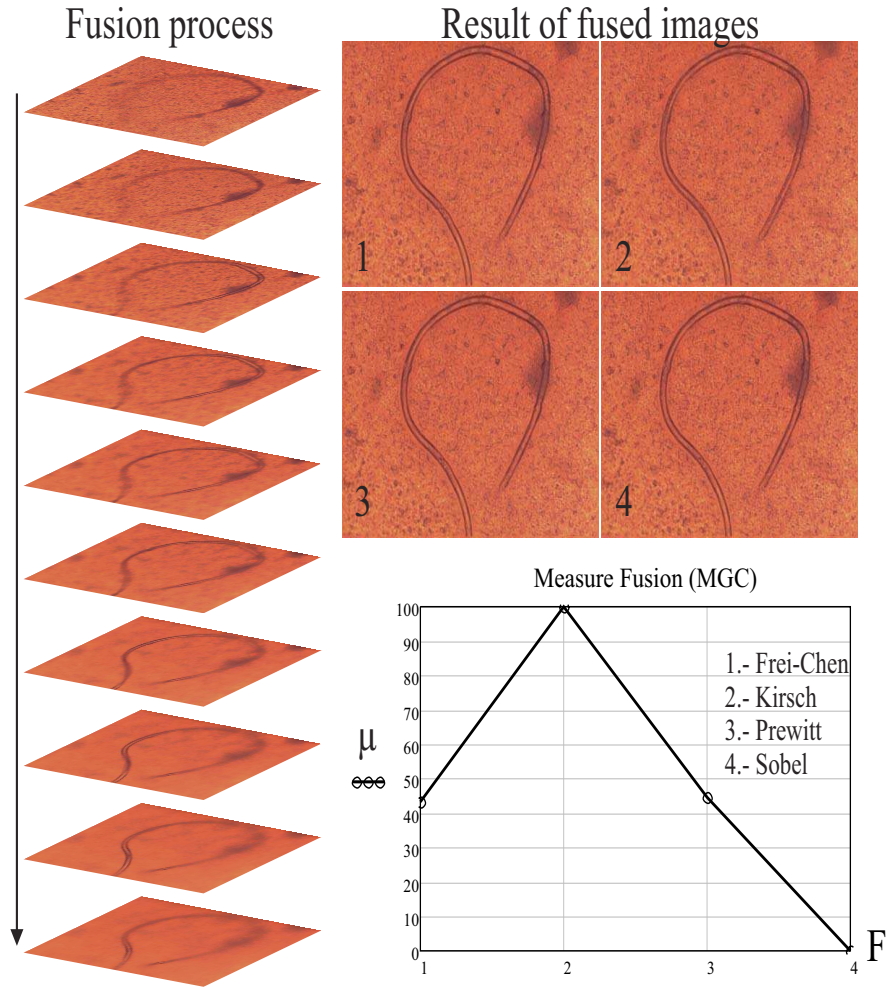


Figure 16. Results of image fusion using the proposed enhancement MGC edge map. The sample is a bacillus of yogurt acquired at $M = 20X$, $N.A. = 0.5$, and an axial distance of $z = 3\mu m$ between the ten focal planes. The results shown that the enhancement MGC edge map with Kirsch filter gives a major contrast fused image.

An image of bee eye is acquired at $M = 10X$, $N.A. = 0.3$, and an axial distance of $z = 10\mu m$ between the four focal planes. The fusion results using

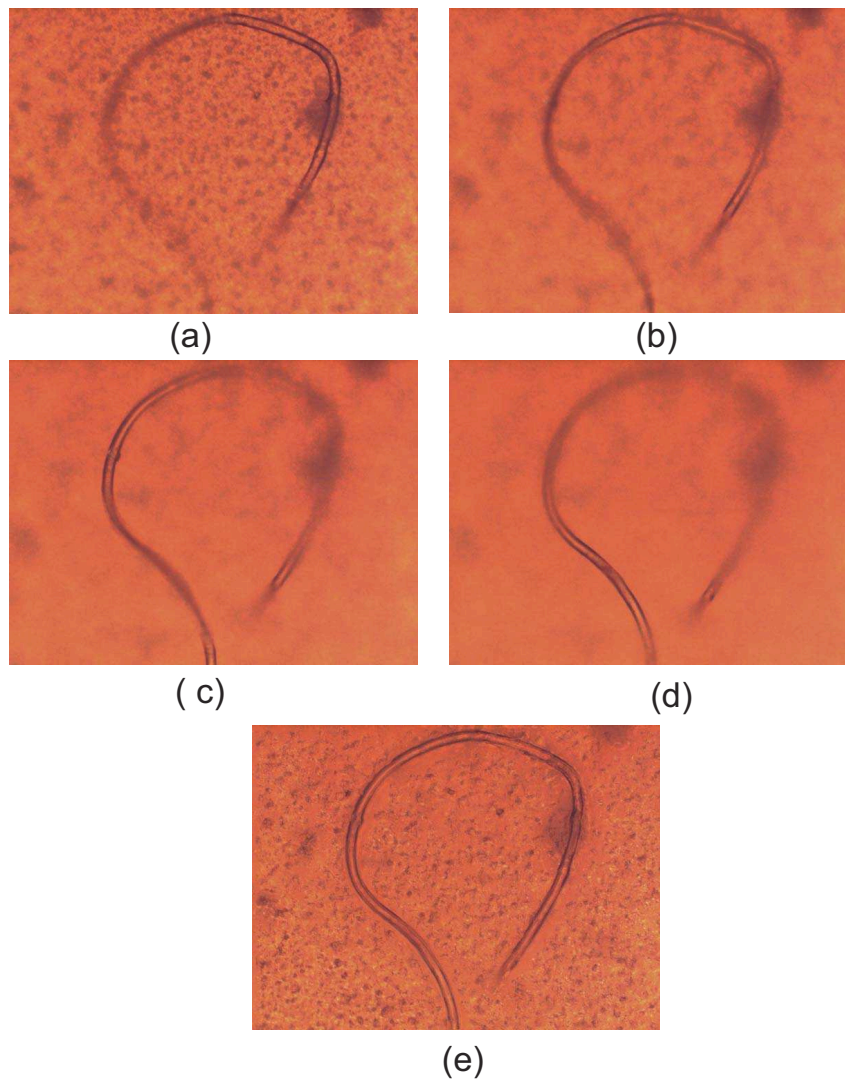


Figure 17. (a) focal plane 1, (b) focal plane 3, (c) focal plane 6 and (d) focal plane 9. Results of image fusion using the proposed enhancement MGC edge map with the sharpening Kirsch filter.

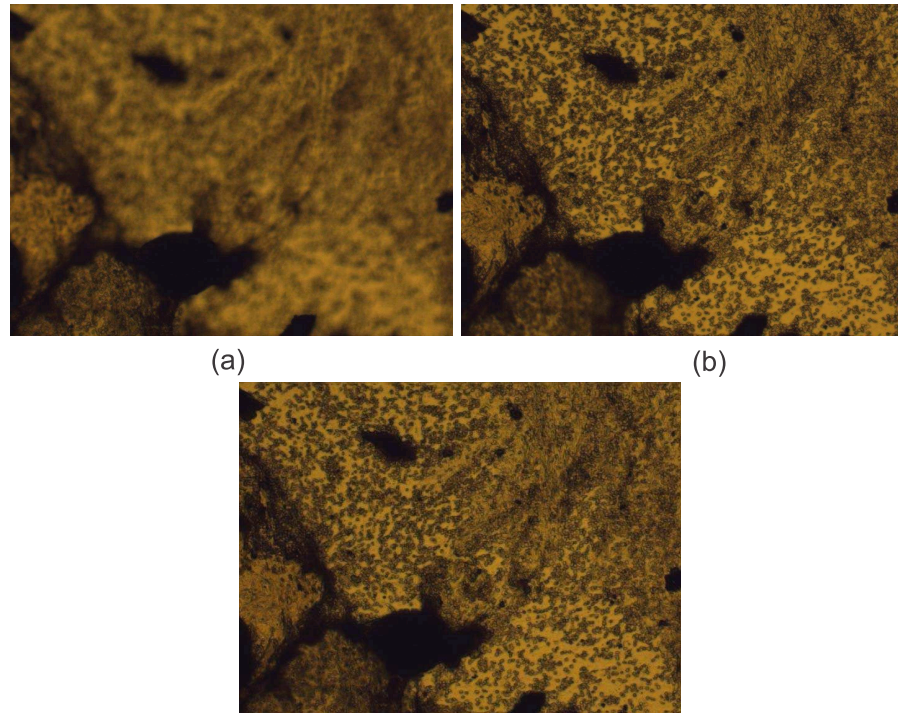


Figure 18. The sample is amniotic fluid. The images are acquired at $M = 10X$, $N.A. = 0.3$, and an axial distance of $z = 10\mu m$ between the two focal planes. (a) focal plane A, (b) focal plane B, and (c) fused image. The results shown that the enhancement *MGC* edge map with Kirsch filter gives a major contrast fused image.

the enhancement *MGC* edge map with different sharpening filters are shown in the Figures 22 and 23. Also a major contrast fused image is obtained using the Kirsch filter.

A stack-image of human tissue is acquired at $M = 2.5X$, $N.A. = 0.16$, and an axial distance of $z = 700\mu m$ between the four focal planes. The fusion results using the enhancement *MGC* edge map with different sharpening filters are shown in the Figures 24 and 25. A major contrast fused image is obtained using the Kirsch filter.

An image of a key is acquired at $M = 2.5X$, $N.A. = 0.16$, and an axial

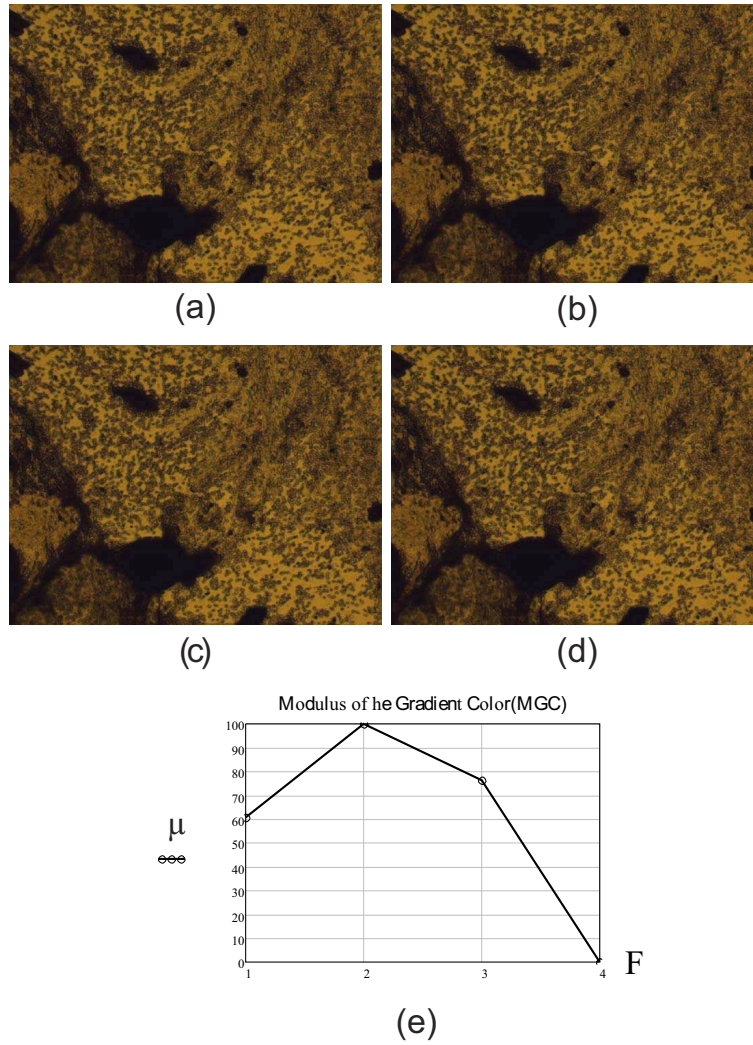


Figure 19. Results of image fusion by means of the proposed enhancement *MGC* edge map with the sharpening filters of (a) Frei-Chen ($F=1$), (b) Kirsch ($F=2$), (c) Prewitt ($F=3$), and (d) Sobel filter ($F=4$). The results show that the enhancement *MGC* edge map with Kirsch filter again gives a major contrast fused image.

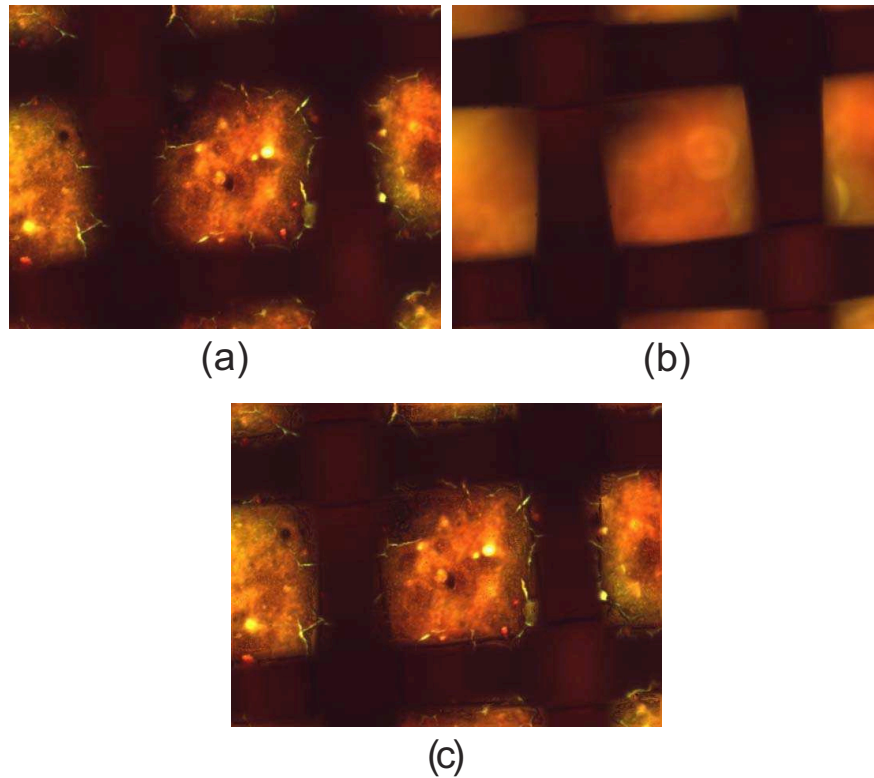


Figure 20. The sample is a tape to measure the glucose levels acquired at $M = 10X$, $N.A. = 0.3$, and an axial distance of $z = 10\mu m$ between the two focal planes. (a) focal plane A, (b) focal plane B, and (c) fused image. The results shown that the enhancement MGC edge map with Kirsch filter gives a major contrast fused image.

distance of $z = 2000\mu m$ between the two focal planes. The fusion results using the enhancement MGC edge map with different sharpening filters are shown in the Figures 26 to 27. A major contrast fused image is obtained using the Kirsch filter.

An image of a metallic key is acquired at $M = 2.5X$, $N.A. = 0.16$, and an axial distance of $z = 2000\mu m$ between the two focal planes. The fusion results using the enhancement MGC edge map with different sharpening filters

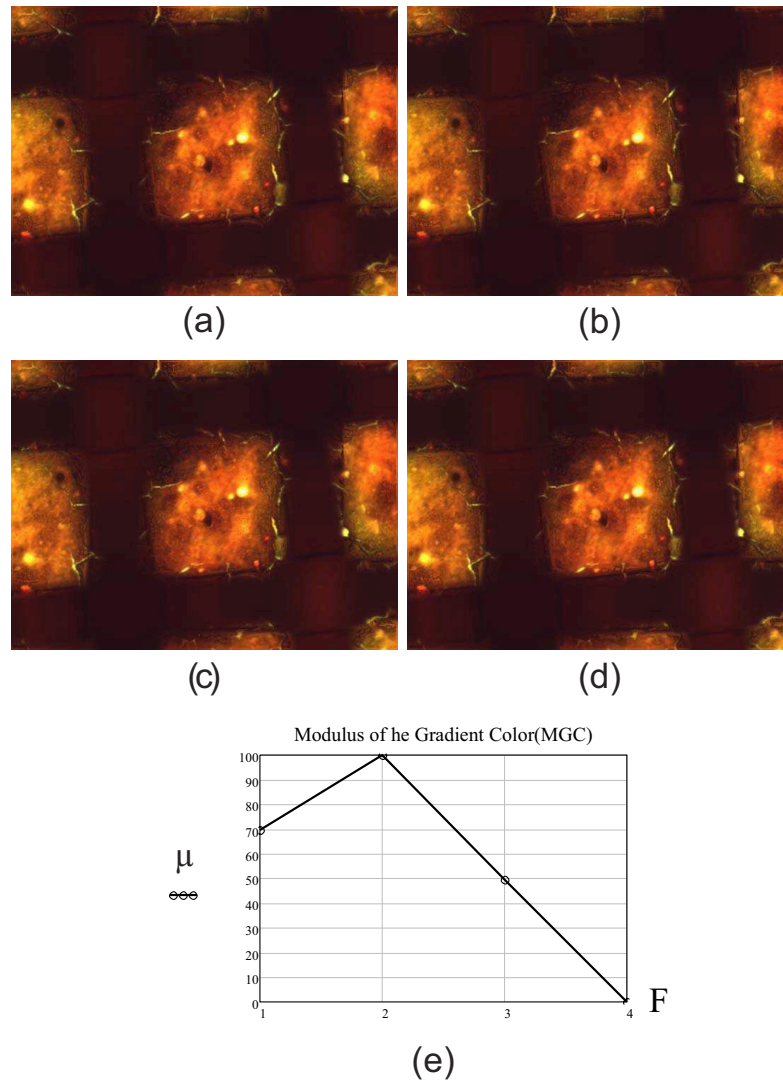


Figure 21. Results of image fusion using the proposed enhancement *MGC* edge map with the sharpening filters of (a) Frei-Chen (F=1), (b) Kirsch (F=2), (c) Prewitt (F=3), and (d) Sobel filter (F=4). The results shown that the enhancement *MGC* edge map with Kirsch filter gives a major contrast fused image.

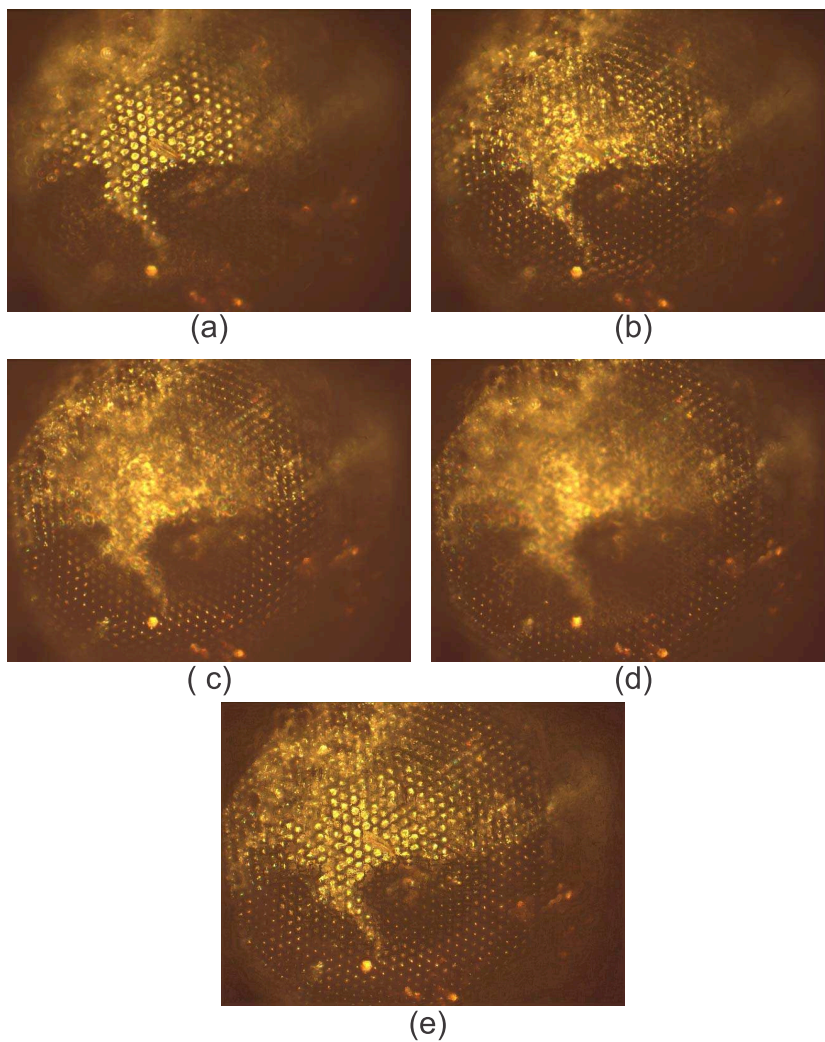


Figure 22. The sample is a bee eye acquired at $M = 10X$, $N.A. = 0.3$, and an axial distance of $z = 10\mu m$ between the four focal planes. (a) focal plane 1, (b) focal plane 2, and (c) focal plane 3, (d) focal plane 4, and (e) fused image. The results shown that the enhancement *MGC* edge map with Kirsch filter gives a major contrast fused image.

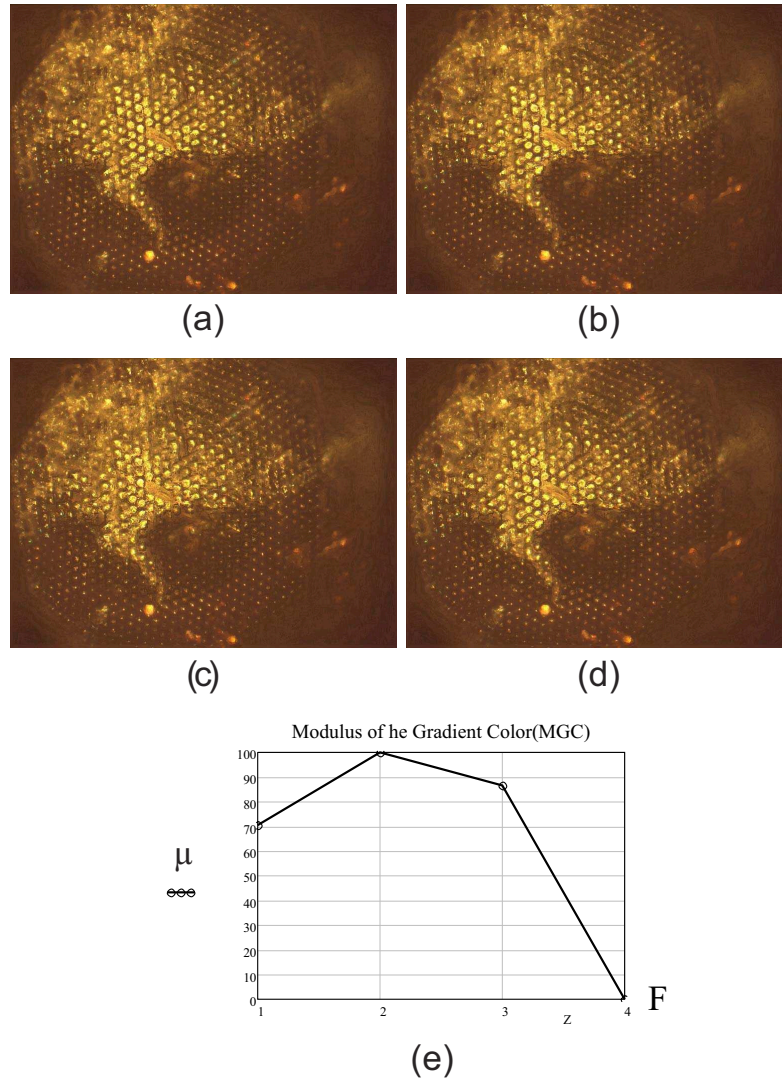


Figure 23. Results of image fusion using the proposed enhancement *MGC* edge map with the sharpening filters of (a) Frei-Chen (F=1), (b) Kirsch (F=2), (c) Prewitt (F=3), and (d) Sobel filter (F=4). The results shown that the enhancement *MGC* edge map with Kirsch filter gives a major contrast fused image.

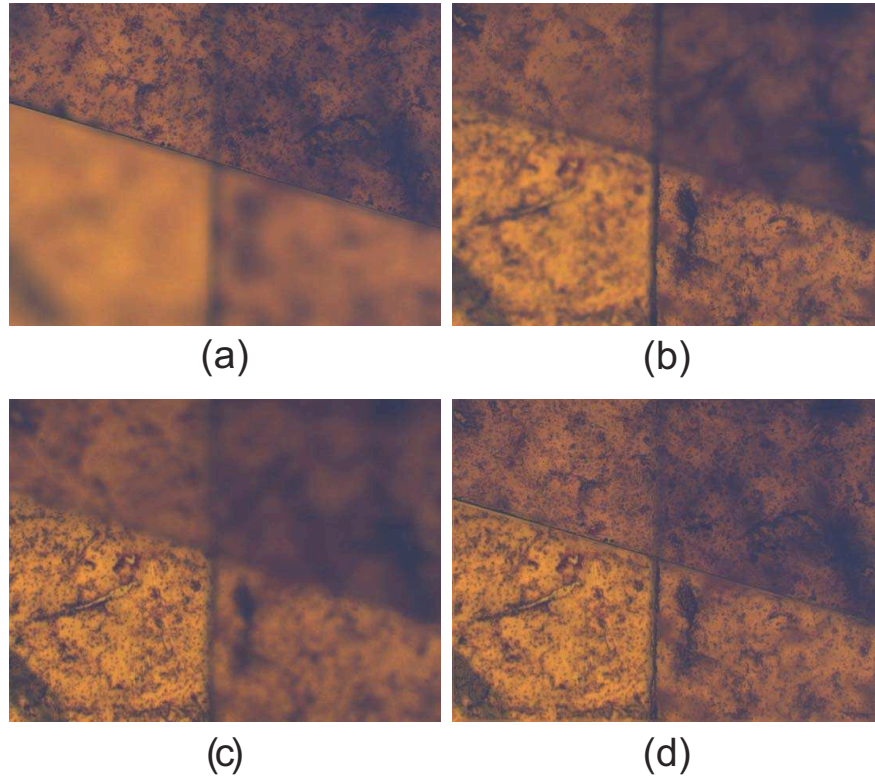


Figure 24. The sample is human tissue acquired at $M = 10X$, $N.A. = 0.3$, and an axial distance of $z = 10\mu m$ between the four focal planes. (a) focal plane 1, (b) focal plane 2, and (c) focal plane 3, (d) focal plane 4, and (e) fused image. The results show that the enhancement *MGC* edge map with Kirsch filter gives a major contrast fused image.

are shown in the Figures 26 to 27. A major contrast fused image is obtained using the Kirsch filter.

6. Discussion and Conclusion

We have presented a novel procedure to extend the *DOF* of a microscopic system. The main contribution of our method is to obtain fused color images with

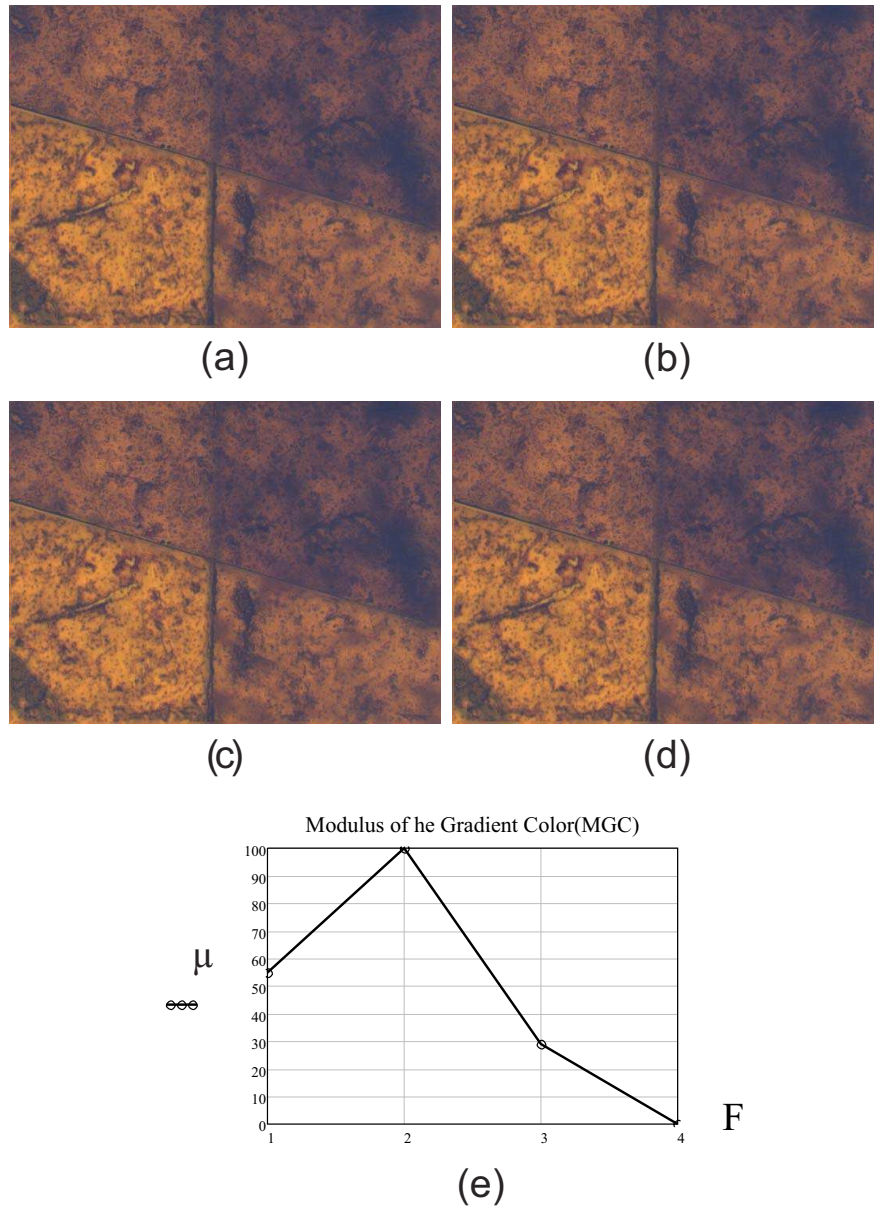


Figure 25. Results of image fusion using the proposed enhancement *MGC* edge map with the sharpening filters of (a) Frei-Chen (F=1), (b) Kirsch (F=2), (c) Prewitt (F=3), and (d) Sobel filter (F=4). The results show that the enhancement *MGC* edge map with Kirsch filter gives a major contrast fused image.

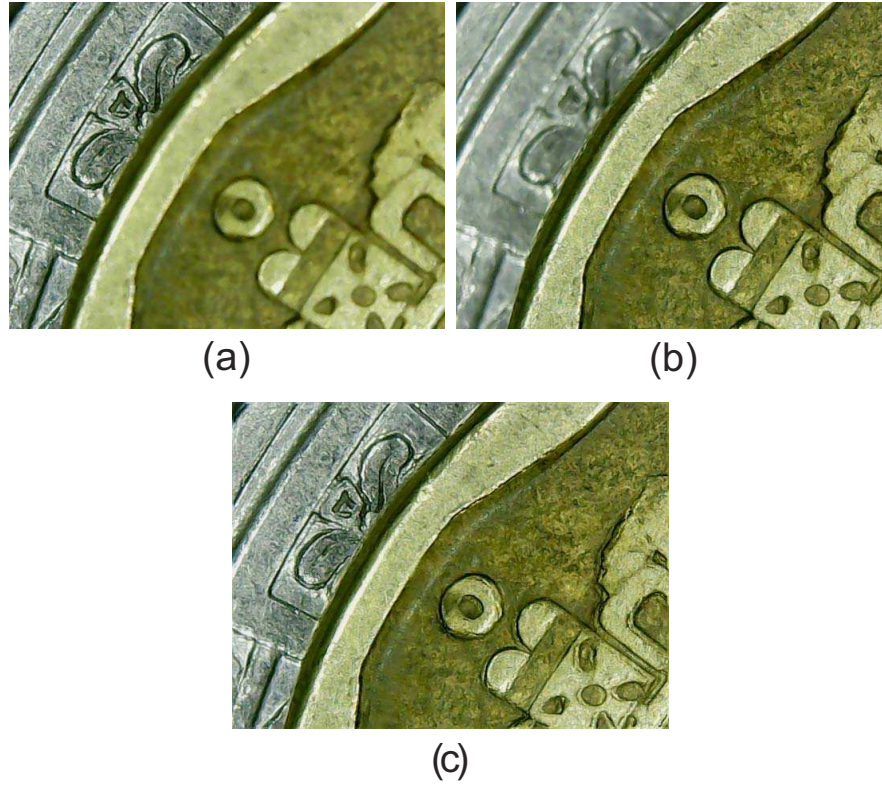


Figure 26. The sample is a metallic key. The image is acquired at $M = 2.5X$, $N.A. = 0.16$, and an axial distance of $z = 2000\mu m$ between the two focal planes. (a) focal plane 1, (b) focal plane 2, and (c) fused image. The results show that the enhancement *MGC* edge map with Kirsch filter gives a major contrast fused image.

high-frequency information from multi-focus color images.

We have proposed the Modulus of the Gradient of the Color planes *MGC*, which is commonly used as an edge detection method. The results shows that, the proposed enhancement *MGC* edge map can be implemented as a fusion scheme of multi-focus color images in the context of microscopy imaging.

Experimental results shows the effectiveness of the proposed method by testing several stacks illuminated with the bright-field technique. Images from

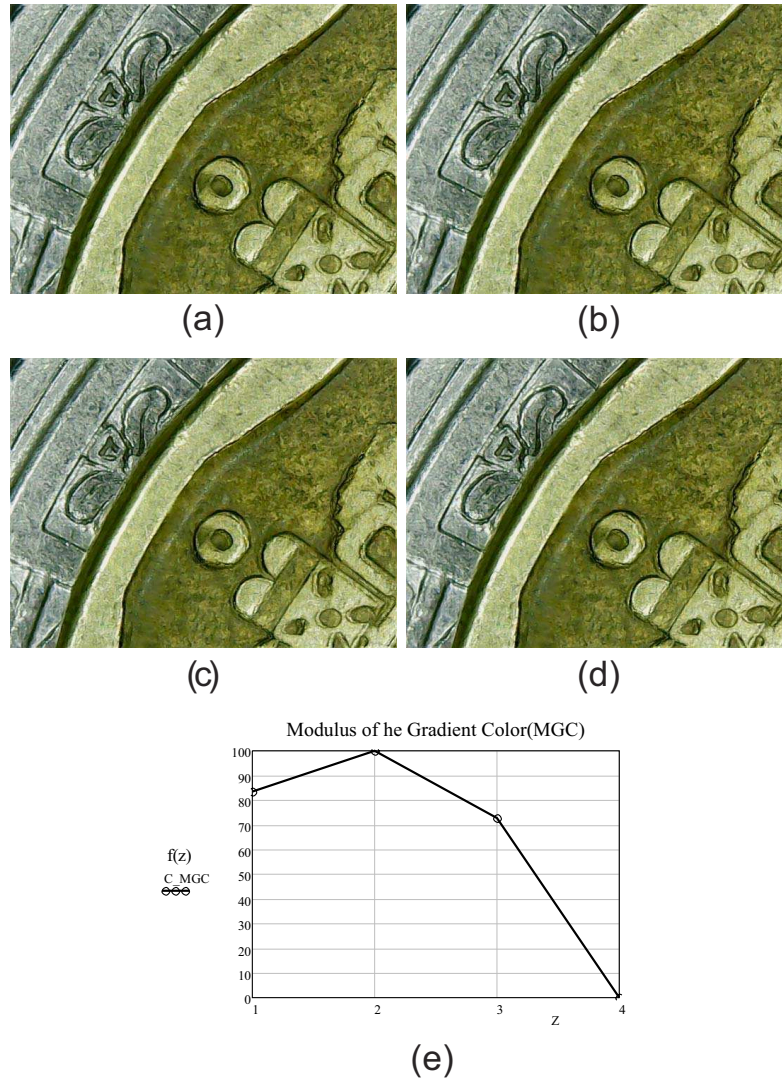


Figure 27. Results of image fusion using the proposed enhancement *MGC* edge map. Using the filters (a) Frei-Chen ($F=1$), (b) Kirsch ($F=2$), (c) Prewitt ($F=3$), and (d) Sobel filter ($F=4$). The results show that the enhancement *MGC* edge map with Kirsch filter gives a major contrast fused image.

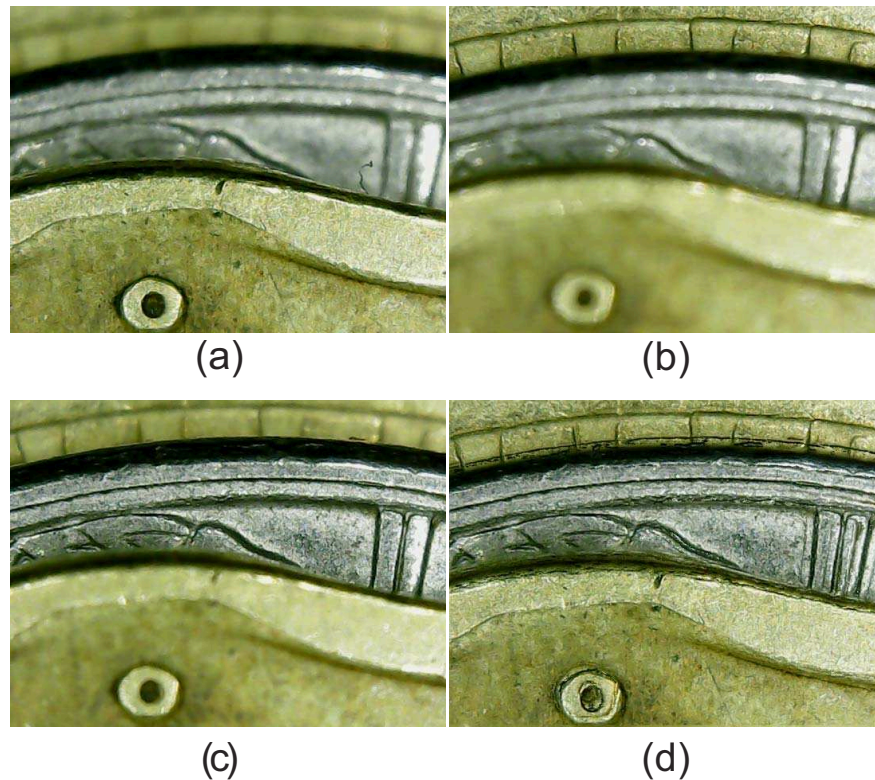


Figure 28. The sample is a key. The image is acquired at $M = 2.5X$, $N.A. = 0.16$, and an axial distance of $z = 2000\mu m$ between the three focal planes. (a) focal plane 1, (b) focal plane 2, (c) focal plane 2, and (d) fused image. The results show that the enhancement *MGC* edge map with Kirsch filter gives a major contrast fused image.

biological and metallic samples have been used to test the performance of the *MGC* algorithm. This *MGC* proposed algorithm is mathematically simple in comparison with other techniques as the wavelet transform. Also, the algorithm is fast to implement because it requires a small number of operations.

According with the qualitative and quantitative results, the final fused image contains the main details or the high frequency information of the multifocus input images. Also, the *MGC* edge map can be used as focus measure, it is

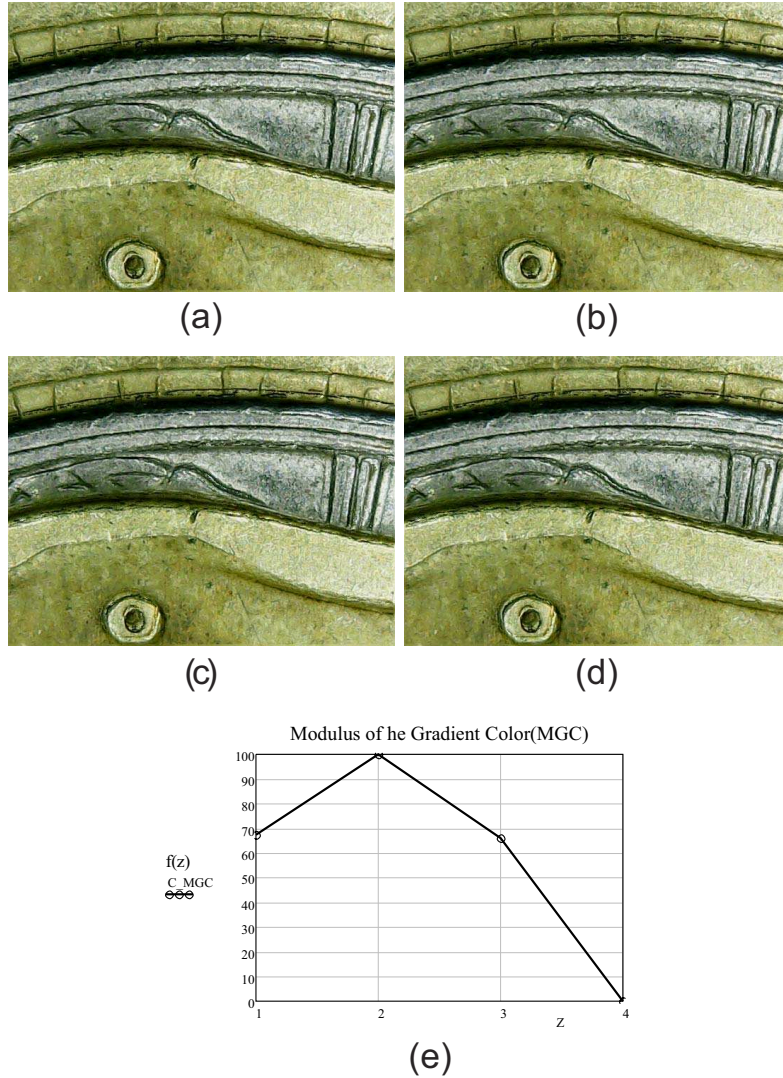


Figure 29. Results of image fusion using the proposed enhancement *MGC* edge map. Using the filters (a) Frei-Chen (F=1), (b) Kirsch (F=2), (c) Prewitt (F=3), and (d) Sobel filter (F=4). The results show that the enhancement *MGC* edge map with Kirsch filter gives a major contrast fused image.

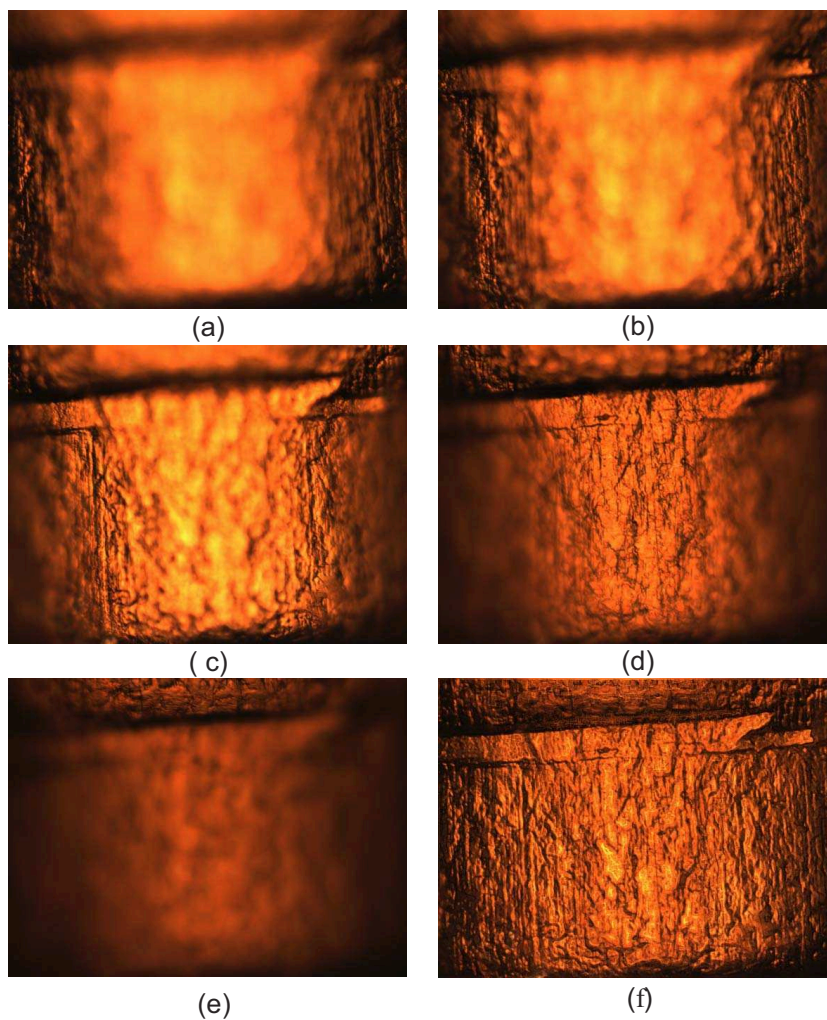


Figure 30. The sample is cylindric piece of metal. The image is acquired at $M = 20X$, $N.A. = 0.5$, and an axial distance of $z = 10\mu m$ between the sixteen focal planes. (a) focal plane 1, (b) focal plane 4, (c) focal plane 8, (d) focal plane 12, (e) focal plane 16, and (f) fused image. The results show that the enhancement *MGC* edge map with Kirsch filter gives a major contrast fused image.

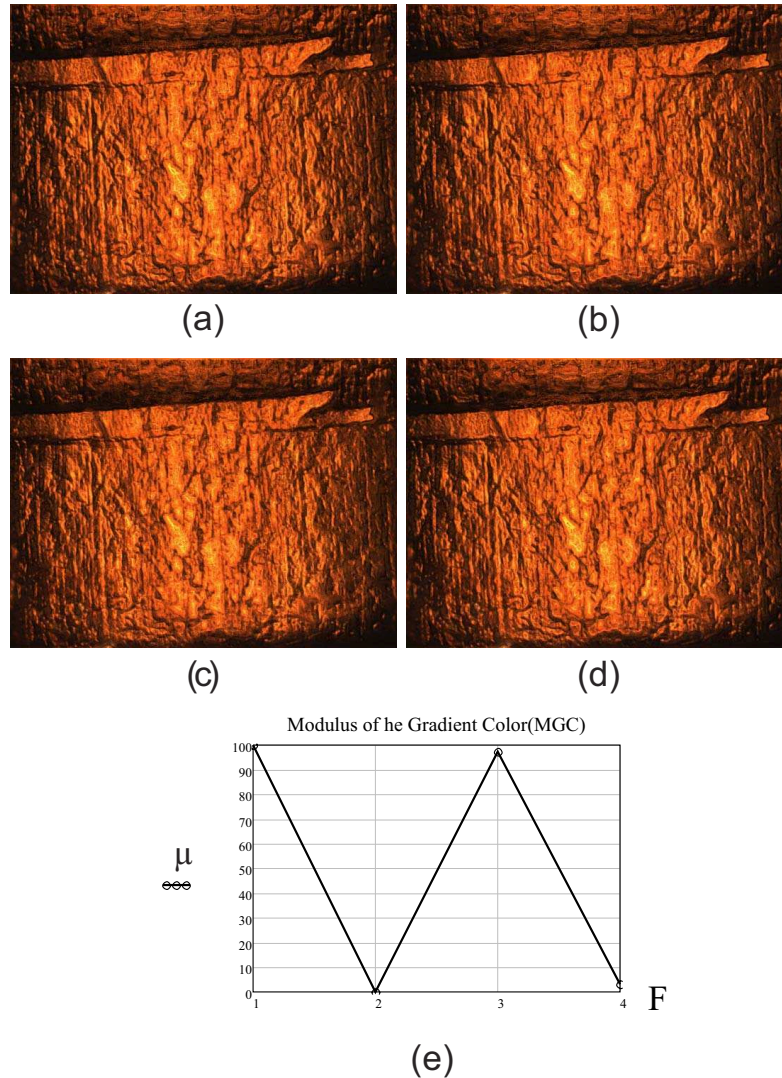


Figure 31. Results of image fusion using the proposed enhancement *MGC* edge map. Using the filters (a) Frei-Chen (F=1), (b) Kirsch (F=2), (c) Prewitt (F=3), and (d) Sobel filter (F=4). The results show that the enhancement *MGC* edge map with Frein-Chen and Kirsch filter gives a major contrast fused image.

also implemented for evaluating the contrast or sharpness of a color final fused image.

Minimum experimental conditions are required to acquire the digital images. Each fused image is obtained from a z - *stack* of multi-focus images which are acquired at the same amplification and the same NA . If the magnification is constant in a specific image fusion using the *MGC* method then the overall fused image does not present artifacts. Additionally, when illumination does not change along a z - *stack* acquisition the fused image results do not present false color. The typical way to get constant illumination in the microscope is by means of a *khöler* illumination system.

One of the important advantage of the proposed fusion method is that, it works for different amplifications of the samples. Practically, good results are obtained for all cases under study.

As preprocessing, we have used four different filters such as Frein-Chen, Kirsch, Sobel and Prewitt over the input images. The interest of taking into account these operations is to enhance input images before the *MGC* planes operator works. With this in mind, the *MGC* algorithm reach a better performance.

We can conclude that, *MGC* method preserves contrast of the input images, it does not generate visible artifacts in the fused image and it is easy-to-implement.

References

- [1] E. R. Dowski and WT Cathey, "Extended depth of field through wavefront coding," *Applied optics*, 34 1859-1866 (1995).
- [2] C. Toxqui-Quitl, Eva Acosta, Justo Arines, and A. Padilla-Vivanco, "Optimized restoration of wavefront coded images," *Proc. SPIE* 9192, Current Developments in Lens Design and Optical Engineering XV, 91921J (2014).
- [3] S. Cheng et al., "An improved method of wavelet image fusion for extended depth-of-field microscope imaging," *Proceeding of the SPIE medical imaging*, 6144 (2006).
- [4] C. Toxqui-Quitl, A. Padilla-Vivanco and G. Urcid-Serrano, "Multifocus image function using the Haar wavelet transform," *Proc. of SPIE* 6748, 555812-112 (2004).

- [5] SA. Sugimoto, and Y. Ichioka, "Digital composition of images with increased depth of focus considering depth information," *Appl Opt* 24, 2076-2080 (1985).
- [6] N. Goldsmith, "Deep focus: a digital image processing technique to produce improved focal depth in light microscopy," *Image Anal. Stereol* 19, 163-167 (2000).
- [7] A. Padilla-Vivanco, I. Tellez-Arteaga, C. Toxqui-Quitl, and C. Santiago-Tepantlan, "Multifocus microscope color imagefusion based on Daub(2) and Daub(4) kernels of the Daubechies Wavelet family," *Proc. SPIE* 7443, (2009).
- [8] J. Nuez, X. Otazu, O. Forse et al, "Multiresolution based image fusion with additive Wavelet decomposition," *IEEE Transactions Geoscience Remote Sensing* 37, 1204-12111 (1999).
- [9] I.T. Young, et al., "Depth of focus in Microscopy," *Proc. of the 8th. Scandinavian Conference on Image Analysis*, 493-498, (1993).
- [10] Guihong Qu, Dali Zhang, Pingfan Yan, "Medical Image Fusion by Wavelet Transform Modulus Maxima". *Optics Express* 4(9), 184-190(2001).
- [11] Ketan Kotwal, Subhasis Chaudhuri, "A novel approach to quantitative evaluation of hyperspectral image fusion techniques," *Information Fusion* 14, 5-18, (2013).
- [12] Shuyuan Yang, Min Wang, Licheng Jiao, " Fusion of multispectral and panchromatic images based on support value transform and adaptive principal component analysis," *Information Fusion* 13, 177-184 (2012).
- [13] Hichem Frigui, Lijun Zhang, Paul Gader, Joseph N. Wilson, K.C. Ho, and Andres Mendez-Vazquez, "An evaluation of several fusion algorithms for anti-tank landmine detection and discrimination," *Information Fusion* 13, 161-174, (2012).
- [14] Shutao Li, James T. Knok, Yaonan Wang, "Using the discrete wavelet frame transform to merge Landsat TM and SPOT panchromatic images," *Information Fusion* 3, 17-23(2002).

- [15] G. Simone, A. Farina, F.C. Morabito, S.B. Serpico, L. Bruzzone, "Image fusion techniques for remote sensing applications," *Information Fusion* 4, 3-15(2002).
- [16] Brigitte Foster, et al., "Complex wavelets for extended depth-of-field: A new method for the fusion of multichannel microscopy images," *Microscopy reseach and technique* 65, 33-42 (2004).
- [17] R. Hurtado-Perez, "Análisis comparativo de algoritmos de enfocamiento en imágenes a color para microscopia optica," *Tesis de Maestria*, Universidad Politecnica de Tulancingo, (2013).
- [18] Theo Gevers, and Harro Stokman, "Classifying color edges in video into shadowgeometry, highlight, or material transitions," *IEEE transactions on multimedia*, 5(2), (2003).
- [19] R. M. Rangayyan, B. Acha, and C. Serrano, "Color image processing with biomedical applications," *SPIE Press*, USA, (2011).
- [20] Andreas Koschan and Mongi Abidi, "Digital color image processing," *Wiley interscience*, USA, (2008).
- [21] Tomasz S. Tkaczyk, "Field guide to Microscopy," *SPIE Field Guides series*, USA (2009).